Research Square

Preprints are preliminary reports that have not undergone peer review.
They should not be considered conclusive, used to inform clinical practice,
or referenced by the media as validated information.

HNRNPC Regulates Autophagy-Related Responses through FOXO1 in Rheumatoid Arthritis Synovial Fibroblast MH7A Cells

Zhipeng Zeng
Nanchang University
Bowen Zheng
Nanchang University
Wen Ye
Nanchang University
Shiyu Gan
Nanchang University
Zhi Wu
Nanchang University
Peng Yu
Nanchang University
Zhongbin Xia
408979872@qq.com
Nanchang University
Shuting Guo
Nanchang University

Research Article

Keywords: HNRNPC, FOXO1, synovial fibroblasts, RNA stability, autophagy, rheumatoid arthritis

Posted Date: November 20th, 2026

DOI: https://doi.org/10.21203/rs.3.rs-11608922/v1

License: This work is licensed under a Creative Commons Attribution 4.0 International License.
Read Full License

Additional Declarations: No competing interests reported.

HNRNPC Regulates Autophagy-Related Responses through FOXO1 in Rheumatoid Arthritis Synovial Fibroblast MH7A Cells

Zhipeng Zeng[1], Bowen Zheng[2], Wen Ye[2], Shiyu Gan[3], Zhi Wu[2], Peng Yu[4†], Zhongbin Xia[5†],Shuting Guo[2]

[1] Department of Rehabilitation Medicine, The Second Affiliated Hospital, Jiangxi Medical College, Nanchang University, Nanchang 330006, Jiangxi, P. R. China

[2] The Second Affiliated Hospital, Jiangxi Medical College, Nanchang University, Nanchang 330006, Jiangxi, P. R. China

[3] Queen Mary School, Nanchang University, Nanchang 330006, Jiangxi, P. R. China

[4] Department of Endocrinology and Metabolism, The Second Affiliated Hospital, Jiangxi Medical College, Nanchang University, Nanchang 330006, Jiangxi, P. R. China

[5] Health Management Center, The Second Affiliated Hospital, Jiangxi Medical College, Nanchang University, Nanchang 330006, Jiangxi, P. R. China

[†]Corresponding authors: Peng Yu and Zhongbin Xia. Correspondence: 408979872@qq.com

Funding: Jiangxi Provincial Science and Technology Department Natural Science Foundation, Youth Fund Project 20242BAB20387.

Abstract

Rheumatoid arthritis (RA) synovial fibroblasts adapt to inflammatory stress, but the post-transcriptional mechanisms linking RNA-binding proteins to autophagy-related responses remain incompletely understood. We investigated whether heterogeneous nuclear ribonucleoprotein C (HNRNPC) regulates these responses through forkhead box O1 (FOXO1) in the human RA synovial fibroblast cell line MH7A. Exploratory public expression analyses were followed by RNA immunoprecipitation, transcript-decay assays, HNRNPC depletion, and FOXO1 rescue experiments. Inflammatory stimulation used tumor necrosis factor-α (20 ng/mL, 48 h). HNRNPC immunoprecipitation enriched FOXO1 RNA, and HNRNPC depletion accelerated FOXO1 transcript decay. HNRNPC depletion also reduced FOXO1, Beclin1, and LC3-II protein abundance. Restoring FOXO1 in HNRNPC-depleted cells increased LC3-II, supporting FOXO1 as a downstream mediator of this response; Beclin1 increased without reaching significance after multiplicity correction. Tandem mCherry-GFP-LC3B images provided qualitative evidence of accompanying reporter changes. HNRNPC depletion increased CCK-8 readings at 12 and 48 h under inflammatory conditions, whereas FOXO1 overexpression reduced readings at 24 h relative to the empty-vector condition. These time-dependent metabolic effects were not shown to depend on autophagy. TNF-α increased FOXO1 transcript abundance despite lower protein abundance, and FOXO1 m6A enrichment did not differ significantly between conditions. Together, the findings support an HNRNPC–FOXO1 regulatory pathway contributing to autophagy-related responses in MH7A cells, alongside context-dependent changes in cellular metabolic activity.

Keywords: HNRNPC; FOXO1; synovial fibroblasts; RNA stability; autophagy; rheumatoid arthritis

1. Introduction

Rheumatoid arthritis (RA) is sustained by interactions between immune cells and the synovial stroma. Fibroblast-like synoviocytes contribute to this process through functions that extend beyond tissue maintenance. Experimental separation of fibroblast populations has shown that inflammatory activity and joint destruction can be mediated by distinct subsets [1]. Single-cell analyses of human synovium have likewise identified fibroblast states associated with inflammatory mediator expression [2]. Endothelium-derived Notch signals help establish fibroblast positional identity, while larger synovial atlases reveal substantial variation in the cellular composition of RA tissue [3, 4]. These findings make fibroblast regulation relevant to RA biology, but also emphasize that individual cellular processes need to be examined before assigning a uniform pathogenic role to a molecular pathway.

Autophagy is one example. In RA fibroblasts, autophagy can help cells adapt to stress, but whether it protects or kills them depends on the stimulus. Kato et al. found that autophagy protected against proteasome-inhibitor-induced apoptosis yet promoted cell death under severe endoplasmic reticulum stress [5]. In TNF-α-stimulated synovial fibroblasts, pharmacological inhibition of autophagy has been reported to increase autophagy-related responses and alter apoptosis [6, 7]. In an anti-TNF treatment study, changes in autophagy and apoptosis in peripheral blood cells were linked to clinical response [8]. These studies link autophagy to inflammatory stress, but how its regulation differs across cellular contexts remains open.

Forkhead box O1 (FOXO1) provides a potential connection between stress-responsive gene regulation and autophagy. In primary RA fibroblasts, inflammatory cytokines were reported to

reduce FOXO1 through a JNK-dependent mechanism involving accelerated transcript decay [9]. In cancer cell models, cytosolic FOXO1 also participates in autophagy through a mechanism involving ATG7 [10]. More recently, PTEN-mediated FOXO signaling was linked to autophagy and other functional responses in RA fibroblast-like synoviocytes [11]. These studies establish that FOXO1 is relevant to fibroblast responses and autophagy; the question addressed here is whether an RNA-binding protein helps control the availability of FOXO1 in an inflammatory synovial fibroblast model.

Heterogeneous nuclear ribonucleoprotein C (HNRNPC) is a plausible candidate: it acts in RNA processing and binds sequence elements whose accessibility can depend on RNA structure. Its suppression of aberrant Alu exon inclusion illustrates how broadly it can affect transcript processing [12]. Liu et al. showed that N6-methyladenosine (m6A) can change local RNA structure and expose HNRNPC-binding sites [13]. Genome-wide maps placed m6A widely across mammalian RNA [14, 15], and studies of YTHDF2 linked m6A recognition to transcript lifetime [16]. These findings justify examining HNRNPC-associated RNA regulation here; they do not imply that every HNRNPC target is m6A-dependent.

In RA, expression-based studies have described m6A-regulator profiles associated with immune signatures and treatment-related differences [17, 18]. Experimental work on an FTO-associated long non-coding RNA pathway has also connected RNA methylation to fibroblast apoptosis-related regulation [19]. However, expression-based candidate selection, RNA association, methylation enrichment, and functional mediation address different levels of evidence. Establishing a regulatory pathway requires connecting an upstream perturbation to a downstream response.

We therefore examined whether HNRNPC regulates autophagy-related responses through FOXO1 in MH7A, an established human RA synovial fibroblast cell line originally generated by SV40 T-antigen immortalization [20]. The experiments first assessed HNRNPC-associated FOXO1 RNA and transcript decay, then tested the consequences of HNRNPC depletion for FOXO1 and autophagy-related proteins. FOXO1 re-expression in the depleted background was used to assess its downstream contribution. Tandem LC3 imaging and CCK-8 measurements provided complementary information about reporter distribution and cellular metabolic activity.

2. Materials and Methods

2.1 Bioinformatics Analysis

GSE93776, comprising 173 expression profiles of sorted peripheral immune cells from patients with RA and healthy donors, was obtained from GEO [21]. This dataset was used for exploratory candidate selection. Expression data for the m6A-associated regulator panel were extracted. Differential expression analysis was performed using the Wilcoxon rank-sum test (screening criteria: $P<0.05$). Protein-protein interaction (PPI) network was constructed using the STRING database (confidence > 0.7) and visualized with Cytoscape software. Random Forest (RF) and Support Vector Machine (SVM) models were built using the "randomForest" and "e1071" packages in R, respectively. Model residual analysis was performed using the "DALEX" package. The importance of feature factors was evaluated by the Mean Decrease Gini index.

Based on the screened differentially expressed m6A regulators, unsupervised consensus clustering of RA samples was performed using the "ConsensusClusterPlus" package to determine

the optimal cluster number and define m6A modification subtypes. An m6A score model was constructed based on principal component analysis (PCA) using the formula: m6A Score=∑(PC1i+PC2i). Differentially expressed genes (DEGs) between different m6A subtypes were identified using the "limma" package [22] (screening criteria: $P<0.05$, $|\log2FC|>0.5$). Gene Ontology (GO) and Kyoto Encyclopedia of Genes and Genomes (KEGG) pathway enrichment analyses were performed using the "clusterProfiler" package.

Expression-signature scores for 28 immune cell types were calculated using single-sample gene set enrichment analysis (ssGSEA). Spearman correlation analysis and Mantel test were used to assess the association among m6A score, HNRNPC expression, and immune infiltration. The intersection of DEGs between RA and normal samples and DEGs between m6A subtypes was obtained. Diagnostic biomarkers were screened via LASSO regression (10-fold cross-validation) and used to construct a nomogram model. The diagnostic efficacy of the model in the training and validation sets was evaluated using receiver operating characteristic (ROC) curves.

2.2 Cell Culture and Inflammatory Stimulation

The human RA synovial fibroblast cell line MH7A was used for all cell-based experiments [20]. Cells were cultured in high-glucose DMEM supplemented with 10% fetal bovine serum and 1% penicillin–streptomycin at 37°C in 5% CO2. Inflammatory stimulation used recombinant human TNF-α at 20 ng/mL for 48 h, with parallel unstimulated controls. The TNF-α concentration series in Fig. 2A assessed IL1B transcript abundance.

2.3 Cell Transfection

Target-specific siRNA screens were performed for HNRNPC and FOXO1. si-HNRNPC #2 and si-FOXO1 #3 were selected from the respective screens. For reporter experiments, cells were transfected with siRNA at a final concentration of 50 nM using Lipofectamine 3000 and incubated for 24 h before TNF-α exposure. FOXO1 overexpression and the corresponding empty-vector control were used for rescue experiments. The rescue groups were siNC, siHNRNPC, siHNRNPC + empty vector, and siHNRNPC + FOXO1 overexpression.

2.4 Quantitative Real-Time PCR (qRT-PCR)

Total RNA was extracted with TRIzol. Reverse transcription used 0.75 μg RNA per reaction with an ABclonal reverse-transcription system. SYBR Green detection was performed on an ABI VII7 instrument. Cycling comprised 95°C for 3 min followed by 40 cycles of 95°C for 5 s and 60°C for 30 s, with melt-curve analysis. Three technical wells were specified per sample. Relative expression was calculated using the $2^{-\Delta\Delta Ct}$ method.

2.5 Western Blot Analysis

For the autophagy-related protein experiments, proteins were extracted using RIPA buffer with PMSF, quantified by BCA, and loaded at 40 μg per lane. After SDS-PAGE and PVDF transfer, membranes were blocked for 60 min. Antibodies included Beclin1 (Affinity, AF5128; 1:1000), FOXO1 (Proteintech, 18592-1-AP; 1:2000), LC3B (Proteintech, 14600-1-AP; 1:4000), and β-actin (Proteintech, 81115-1-RR; 1:20000). Detection used an IRDye 680RD goat anti-rabbit secondary antibody (LI-COR, 925-68071) and an Odyssey imaging system. Signals were quantified in ImageJ. Each target signal was divided by the corresponding β-actin signal, then by the mean control-group ratio across the three replicate records. LC3-II was normalized to β-actin; an LC3-II/LC3-I ratio was not calculated.

2.6 RNA Immunoprecipitation (RIP)

The Magna RIP RNA-Binding Protein Immunoprecipitation Kit was used. Approximately 1×10^7 MH7A cells were collected and lysed with RIP lysis buffer. 10% of the lysate was saved as Input control. The remaining lysate was incubated overnight at 4°C with magnetic beads coated with anti-HNRNPC antibody or control IgG. After washing, the immunoprecipitated complexes were digested with Proteinase K. RNA was extracted and subjected to qRT-PCR to detect the relative enrichment of FOXO1 mRNA in the immunoprecipitated products.

2.7 m6A Methylated RNA Immunoprecipitation (MeRIP-qPCR)

FOXO1 RNA enrichment was measured after immunoprecipitation with an anti-m6A antibody, with IgG and input controls. Enrichment was reported as a percentage of input. Control and TNF-α-stimulated cells were compared.

2.8 mRNA Stability Assay (Actinomycin D Experiment)

FOXO1 transcript decay after HNRNPC depletion was examined using actinomycin D, with samples collected at 0, 2, 4, 6, and 8 h. Remaining FOXO1 RNA was expressed relative to the 0-h value.

2.9 Cellular Metabolic Activity Assay (CCK-8)

MH7A cells were seeded into 96-well plates at a density of 5×10^3 cells per well. After the respective treatments, 10 μL of CCK-8 solution was added to each well, followed by incubation at 37°C for 2 h. Absorbance at 450 nm was measured using a multimode microplate reader. Five independent experiments were analyzed per group and time point. Blank-corrected readings were normalized to the corresponding baseline-group mean. The assay was used to assess cellular metabolic activity. The assay is based on WST-8 reduction [23].

2.10 Tandem mCherry-GFP-LC3B Reporter Imaging

Cells were seeded and transduced with tandem Ad-mCherry-GFP-LC3B adenovirus (Beyotime, C3011) at an MOI of 30 for 36–48 h. Cells were subsequently transfected with siRNA at a final concentration of 50 nM and incubated for 24 h, followed by TNF-α treatment (20 ng/mL, 48 h). Cells were then fixed with 4% paraformaldehyde for 15 min, washed, and imaged by confocal microscopy. GFP and mCherry channels were acquired and merged. Yellow puncta indicate overlapping GFP and mCherry signals; red-only puncta are consistent with reporter delivery into acidic compartments. Total puncta alone were not interpreted as a flux rate. Reporter interpretation followed the tandem-LC3 principle described previously [24].

2.11 Statistical Analysis

Western blot results are presented as mean ± SD from three independent biological experiments. Each experiment included all four conditions and involved independent plating, treatment, and sample collection. Protein signals were normalized to β-actin and then to the mean control value. The same experimental run supplied the matched observations for two-sided paired t tests. Holm correction was applied across all six pairwise comparisons for each protein within each WB experiment. CCK-8 data were obtained from five independent experiments per group and time point. For CCK-8, two-sided Welch t tests compared two specified group pairs at each of four time points, with Holm correction across eight comparisons per panel. All five values in the source dataset were retained, including a negative blank-corrected value. No cross-condition

pairing was assumed for CCK-8. Exact adjusted P values and descriptive statistics are supplied in Supplementary Statistical Tables. The small number of WB experiments limits assessment of distributional assumptions. No inferential statistics were assigned to the representative LC3 reporter images.

3. Results

3.1 Exploratory Public Expression Analysis Prioritizes HNRNPC

Exploratory analysis of the public expression dataset identified HNRNPC among differentially expressed m6A-associated regulators (Fig. 1). Co-expression, STRING network, and random-forest analyses were used to prioritize candidates. These analyses reflect expression associations; STRING edges do not establish interactions demonstrated in the MH7A experiments.

HNRNPC ranked highly in the random-forest analysis (Fig. 1D; Fig. S1). The classification, nomogram, and calibration results were obtained within the public-data analysis and were interpreted as exploratory rather than as evidence of clinical diagnostic utility.

Consensus clustering separated expression-defined groups with different regulator-expression profiles (Fig. S2). These groups were termed m6A-regulator expression clusters; expression-based clustering does not directly measure transcriptome-wide m6A modification.

Functional enrichment and ssGSEA identified differences in immune-related expression signatures between clusters (Fig. S2; Fig. 4D). These scores describe transcriptomic patterns in the public dataset.

Additional classification results are shown in Fig. S3. Together, the exploratory analyses provided a rationale for examining HNRNPC in the cell model.

Fig. 1. Exploratory public expression analysis prioritizes HNRNPC in RA

(A) Correlations and expression profiles of m6A-associated regulators. (B) Differential expression between RA and control samples. (C) STRING association network. (D) Random-forest feature importance. (E) Expression heatmap. (F) Expression-derived m6A-regulator scores and immune-related signatures. Public-data analyses were exploratory; scores do not directly measure RNA methylation or cell infiltration.

3.2 TNF-α Alters HNRNPC and FOXO1 Expression

IL1B transcript abundance increased in the TNF-α concentration series (Fig. 2A). Subsequent inflammatory stimulation used 20 ng/mL TNF-α for 48 h. HNRNPC transcript abundance was higher in model cells than in controls (Fig. 2B, E). The concentration series was not used to infer an HNRNPC-specific optimum.

TNF-α stimulation increased FOXO1 transcript abundance (Fig. 2D), whereas the independent protein measurements showed lower FOXO1 abundance in model cells than in controls (Fig. 4C). Anti-m6A immunoprecipitation enriched FOXO1 RNA relative to IgG in both conditions, with no significant control–model difference (Fig. 2F).

Fig. 2. HNRNPC and FOXO1 transcript expression and FOXO1 m6A enrichment

(A) IL1B transcript abundance across the TNF-α concentration series. (B) HNRNPC transcript abundance in control and model cells. (C) Electrophoretic images from the RNA-assay workflow.

(D, E) FOXO1 and HNRNPC transcript abundance, respectively. (F) FOXO1 RNA enrichment in anti-m6A and IgG immunoprecipitates, expressed as percentage of input. FOXO1 RNA was enriched relative to IgG in both conditions, without a significant control–model difference in the analysis. Model stimulation was 20 ng/mL TNF-α for 48 h.

3.3 HNRNPC Associates with FOXO1 RNA and Supports Transcript Stability

FOXO1 RNA was enriched in anti-HNRNPC immunoprecipitates relative to IgG (Fig. 3A), placing FOXO1 RNA in an HNRNPC-associated complex.

The separate FOXO1 and HNRNPC siRNA screens are shown in Fig. 3B and C, respectively. si-FOXO1 #3 and si-HNRNPC #2 were selected for the corresponding experiments.

FOXO1 RNA declined more rapidly after transcriptional inhibition in HNRNPC-depleted cells than in controls (Fig. 3F). The time course is consistent with a contribution of HNRNPC to FOXO1 transcript stability. Amplification and melting curves are shown in Fig. 3D and E, respectively.

Fig. 3. HNRNPC-associated FOXO1 RNA and transcript decay

(A) FOXO1 RNA enrichment in anti-HNRNPC and IgG immunoprecipitates. (B) FOXO1-targeting siRNA screen. (C) HNRNPC-targeting siRNA screen. Panels B and C include protein and transcript measurements. si-FOXO1 #3 and si-HNRNPC #2 were selected from their respective screens. (D, E) qPCR amplification and melting curves. (F) FOXO1 RNA remaining at 0, 2, 4, 6, and 8 h after transcriptional inhibition in control and HNRNPC-depleted cells.

3.4 HNRNPC Depletion Alters Autophagy-Related Responses and Cellular Metabolic Activity

Representative tandem LC3 images showed differences in reporter distribution following TNF-α stimulation and HNRNPC depletion (Fig. 4A). These images were assessed qualitatively. Model cells showed higher Beclin1 and LC3-II abundance but lower FOXO1 abundance than controls. HNRNPC depletion reduced Beclin1, FOXO1, and LC3-II relative to model + siNC, with Holm-adjusted paired-test P values of 0.0147, 0.0400, and 0.00999, respectively (Fig. 4C).

CCK-8 measurements varied with treatment and time (Fig. 4B). In the inflammatory-stimulation panel, the HNRNPC-depleted group had higher readings than the model + siNC group at 12 h (Holm-adjusted $P = 0.00155$) and 48 h ($P = 0.00000736$), but not at 24 h ($P = 0.125$). In the second panel, HNRNPC depletion alone did not differ significantly from siNC after correction. FOXO1 overexpression reduced the CCK-8 reading relative to the empty-vector condition at 24 h ($P = 0.0420$), whereas the comparisons at 12 and 48 h were not significant after correction. These measurements reflect cellular metabolic activity and do not establish proliferation or invasion. The ssGSEA results in Fig. 4D were analyzed separately from the cell experiments.

Fig. 4. LC3 reporter patterns, cell metabolic activity, and protein responses to HNRNPC depletion

(A) Representative tandem mCherry-GFP-LC3B reporter images. Images are qualitative; no puncta-count statistics were performed. (B) CCK-8 time courses for inflammatory stimulation and FOXO1 overexpression experiments, redrawn from the source values. Points show mean ± SD, n = 5 independent experiments. Readings were blank-corrected and normalized to the corresponding baseline-group mean. The negative blank-corrected observation was retained.

CCK-8 comparisons used two-sided Welch t tests with Holm correction across eight tests per panel; exact P values are in Supplementary Statistical Tables. (C) Representative immunoblots and protein quantification, mean ± SD with individual observations, n = 3 independent experiments. Each run included all four groups. Target signals were normalized to β-actin and then to the mean control value. The displayed P values compare model + siNC with model + siHNRNPC using paired t tests with Holm correction across six pairs per protein. (D) Public-data ssGSEA signature scores. siHNRNPC denotes si-HNRNPC #2. TNF-α: 20 ng/mL for 48 h.

3.5 FOXO1 Rescue Supports Its Position Downstream of HNRNPC

To test whether FOXO1 mediates the autophagy-related effects of HNRNPC depletion, FOXO1 was re-expressed in HNRNPC-depleted MH7A cells. FOXO1 protein abundance increased relative to the HNRNPC-depleted empty-vector group (Holm-adjusted P = 0.0364), confirming restoration of the downstream factor. LC3-II abundance also increased (P = 0.0466). Beclin1 changed in the same direction, although the comparison did not reach significance after correction (P = 0.0690; Fig. 5B). Thus, FOXO1 restoration partially reversed the protein changes associated with HNRNPC depletion.

Representative tandem LC3 images showed accompanying changes in reporter distribution after FOXO1 restoration (Fig. 5A). The rescue results, considered with the RNA-association and transcript-decay experiments, support FOXO1 as a downstream functional mediator of the HNRNPC-dependent autophagy-related response. CCK-8 results showed a reduction after FOXO1 restoration at 24 h (Fig. 4B), but not at the other tested times after correction. The experiments therefore establish a partial rescue of autophagy-related readouts rather than a uniform rescue of cellular metabolic activity.

Fig. 5. FOXO1 restoration partially reverses the autophagy-related effects of HNRNPC depletion

(A) Representative tandem mCherry-GFP-LC3B images in siNC, siHNRNPC, siHNRNPC + empty vector, and siHNRNPC + FOXO1-overexpressing cells. Images were assessed qualitatively without puncta-count statistics. (B) Representative immunoblots and quantification of Beclin1, FOXO1, and LC3-II. Signals were normalized to β-actin and expressed relative to the mean siNC ratio. Bars show mean ± SD with individual observations from three independent experiments, each containing all four groups. The displayed P values compare the empty-vector and FOXO1-overexpressing conditions using two-sided paired t tests with Holm correction across all six pairs per protein. Beclin1 did not reach significance after correction. siHNRNPC denotes si-HNRNPC #2. TNF-α: 20 ng/mL for 48 h.

4. Discussion

This study identifies a post-transcriptional connection between HNRNPC and FOXO1 that contributes to autophagy-related responses in MH7A cells. The evidence follows a functional sequence: FOXO1 RNA was enriched in HNRNPC immunoprecipitates; HNRNPC depletion accelerated FOXO1 transcript decay and reduced FOXO1 protein abundance; and FOXO1 re-expression increased LC3-II in the HNRNPC-depleted background. The rescue result is central because it connects the RNA-regulatory observations to a downstream protein response. It supports a partial contribution of FOXO1 to the effects of HNRNPC depletion, with Beclin1 showing a directionally similar but statistically non-significant recovery after correction.

4.1 HNRNPC–FOXO1 Regulation in the Context of RA Fibroblast Biology

Previous studies already place FOXO1 within the biology of RA fibroblasts. Grabiec and colleagues showed cytokine-induced FOXO1 downregulation through JNK-dependent transcript destabilization in primary RA fibroblasts [9]. Chen and colleagues subsequently linked PTEN-mediated FOXO signaling to autophagy and functional responses in RA fibroblast-like synoviocytes [11]. The contribution of the present study is therefore the identification of HNRNPC-associated regulation of FOXO1 RNA, coupled with a rescue experiment supporting FOXO1 involvement downstream of HNRNPC. This extends the upstream regulatory context of FOXO1 rather than treating the connection between FOXO1 and autophagy itself as a new observation.

The public expression analysis provided a route to candidate selection. GSE93776 contains profiles of sorted peripheral immune cells from the study of molecular responses to RA treatment by Tasaki and colleagues [21]; it is not a synovial fibroblast dataset. Thus, its HNRNPC signal supplies a disease-associated expression context, whereas the regulatory relationship reported here was tested in MH7A cells. This distinction matters because both blood-cell composition and synovial-cell heterogeneity can influence expression signatures [21, 4]. The classifiers and expression-defined clusters should consequently be regarded as exploratory, without attributing their signals specifically to synovial fibroblasts or claiming diagnostic performance in clinical practice.

4.2 Transcript Stability and the Interpretation of m6A Enrichment

The RIP and decay experiments address different parts of the same question. RIP shows that FOXO1 RNA is present in an HNRNPC-containing complex. After HNRNPC depletion, FOXO1 RNA declined faster when transcription was blocked, suggesting that HNRNPC helps maintain FOXO1 transcript levels. HNRNPC acts broadly on RNA processing; one example is its suppression of aberrant Alu exon inclusion [12]. The decay phenotype may therefore arise from direct regulation of FOXO1 RNA or from effects on other RNA-processing components. These experiments establish a regulatory relationship; they do not identify the contact site or the molecular composition of the complex.

The m6A result also requires a distinction between the presence of a modification and dependence on it. FOXO1 RNA was enriched by anti-m6A immunoprecipitation in both control and stimulated cells, with no significant difference between conditions. HNRNPC can respond to m6A-induced structural accessibility, as demonstrated by the m6A-switch mechanism [13]; however, that mechanism cannot be assigned to FOXO1 solely from RIP and MeRIP enrichment. An unchanged enrichment measurement neither demonstrates methylation-dependent regulation nor excludes a role for specific sites that were not resolved by the assay. Accordingly, the supported mechanism is HNRNPC-associated control of FOXO1 transcript stability, while m6A dependence remains an open molecular question.

4.3 FOXO1 Rescue Connects RNA Regulation to Autophagy-Related Responses

The depletion and rescue experiments support a downstream position for FOXO1. HNRNPC depletion reduced FOXO1, Beclin1, and LC3-II in the inflammatory model. Re-expression of FOXO1 then increased LC3-II relative to the depleted empty-vector group. This reversal argues that reduced FOXO1 availability contributes to the LC3-II response after HNRNPC depletion. The Beclin1 estimate changed in the same direction, but its adjusted P value of 0.0690 does not

establish recovery of that marker. Thus, the rescue supports a FOXO1-dependent component of the response without implying that all consequences of HNRNPC depletion are transmitted through FOXO1.

The biological route from FOXO1 to autophagy can itself vary. Zhao and colleagues demonstrated a cytosolic FOXO1–ATG7 mechanism in stressed cancer cells [10], whereas the present experiments measured total FOXO1 abundance without determining its localization, acetylation, or transcriptional activity. The results should therefore not be assigned to a particular FOXO1 effector mechanism. Their contribution is to place FOXO1 between HNRNPC perturbation and an autophagy-related protein response in MH7A cells.

LC3-II and tandem LC3 imaging also describe different aspects of the pathway. LC3-II associates with autophagosome membranes [25], and tandem reporters exploit the different responses of green and red fluorophores to acidic compartments [24]. These properties make the reporter images informative alongside the protein measurements. However, endpoint LC3-II abundance can reflect changes in formation, clearance, or both, and representative images without puncta quantification do not supply a rate of degradation. Following established assay-interpretation guidance [26], the present observations support changes in autophagy-related responses rather than a quantified increase or decrease in degradative flux.

4.4 Transcript–Protein Discordance and the Cellular Metabolic Phenotype

TNF-α increased FOXO1 transcript abundance while the independent protein experiment showed lower FOXO1 abundance. The transcript result differs from the rapid cytokine-associated downregulation reported in primary RA fibroblasts [9]. An immortalized line, distinct sampling conditions, and the time course of the response may contribute to the difference, but these explanations were not tested. More importantly, the control–TNF-α comparison represents the net response to inflammatory stimulation, whereas the depletion–rescue comparison examines the contribution of HNRNPC within the experimental model. HNRNPC can help maintain FOXO1 availability even when the net effect of TNF-α on FOXO1 protein is downward; the results do not require TNF-α to raise FOXO1 at both transcript and protein levels.

The CCK-8 results show that the cellular phenotype did change. Under inflammatory stimulation, HNRNPC depletion increased readings at 12 and 48 h, while the 24-h comparison was not significant after correction. In the second panel, depletion alone did not differ significantly from siNC, and FOXO1 re-expression reduced the reading relative to the empty-vector group at 24 h. WST-8 reduction provides an assay of viable-cell-associated metabolic activity [23]; it does not independently identify proliferation, apoptosis, or inflammatory output. The time-dependent pattern therefore argues against describing HNRNPC as uniformly promoting or suppressing cell growth.

The simultaneous reduction in autophagy-related proteins and increase in CCK-8 readings is biologically relevant, even though it does not establish a causal connection between the two. The dual effects of autophagy on RA fibroblast death under different stresses provide precedent for avoiding a fixed pro-survival interpretation [5]. Studies showing survival-associated autophagy after TNF-α exposure used additional interventions and apoptosis measurements [6, 7]. Those findings supply context but cannot determine the direction of the phenotype in the present experiments. Here, the strongest functional conclusion concerns FOXO1-dependent restoration of LC3-II; the metabolic response is an accompanying, context-dependent observation.

4.5 Disease Relevance and Study Limitations

The RA relevance of these findings lies in the regulation of a stress-responsive pathway in a disease-derived fibroblast model. Autophagy-related changes have been associated with treatment response in RA blood cells [8], while synovial studies show that fibroblast identity and inflammatory functions depend on tissue context [1, 3, 4]. The present results add an upstream RNA-regulatory relationship to this framework. They do not establish whether targeting HNRNPC would reduce synovitis, because cytokine output after HNRNPC depletion and FOXO1 rescue was not measured. A therapeutic direction cannot be inferred from the autophagy-related markers alone.

Several limitations define the scope of the conclusion. All cell experiments used MH7A, whose immortalization and growth properties differ from those of parental fibroblasts [20]; primary patient-derived cells and animal models were not included. Three independent WB experiments provide limited precision. The reporter images were qualitative, the RNA assays did not map direct contact or methylation-dependent sites, and forced FOXO1 expression may bypass endogenous regulation. Nevertheless, the combined RNA-association, decay, depletion, and rescue experiments support a coherent HNRNPC–FOXO1 regulatory relationship. The evidence is strongest for its contribution to autophagy-related protein responses in this cellular model.

5. Conclusion

HNRNPC supports FOXO1 transcript stability and regulates autophagy-related responses at least partly through FOXO1 in the RA synovial fibroblast cell line MH7A. FOXO1 re-expression partially reverses the effects of HNRNPC depletion, supporting its position as a downstream functional mediator. HNRNPC depletion also alters cellular metabolic activity in a time- and context-dependent manner.

References

1. Croft AP, Campos J, Jansen K, Turner JD, Marshall J, Attar M, et al. Distinct fibroblast subsets drive inflammation and damage in arthritis. Nature. 2019;570(7760):246-251. https://doi.org/10.1038/s41586-019-1263-7

2. Zhang F, Wei K, Slowikowski K, Fonseka CY, Rao DA, Kelly S, et al. Defining inflammatory cell states in rheumatoid arthritis joint synovial tissues by integrating single-cell transcriptomics and mass cytometry. Nat Immunol. 2019;20(7):928-942. https://doi.org/10.1038/s41590-019-0378-1

3. Wei K, Korsunsky I, Marshall JL, Gao A, Watts GFM, Major T, et al. Notch signalling drives synovial fibroblast identity and arthritis pathology. Nature. 2020;582(7811):259-264. https://doi.org/10.1038/s41586-020-2222-z

4. Zhang F, Jonsson AH, Nathan A, Millard N, Curtis M, Xiao Q, et al. Deconstruction of rheumatoid arthritis synovium defines inflammatory subtypes. Nature. 2023;623(7987):616-624. https://doi.org/10.1038/s41586-023-06708-y

5. Kato M, Ospelt C, Gay RE, Gay S, Klein K. Dual role of autophagy in stress-induced cell death in rheumatoid arthritis synovial fibroblasts. Arthritis Rheumatol. 2014;66(1):40-48. https://doi.org/10.1002/art.38190

6. Dai Y, Ding J, Yin W, He Y, Yu F, Ye C, et al. Increased Autophagy Enhances the Resistance to Tumor Necrosis Factor-Alpha Treatment in Rheumatoid Arthritis Human Fibroblast-Like Synovial Cell. Biomed Res Int. 2018;2018:4941027. https://doi.org/10.1155/2018/4941027

7. Wang Y, Gao W. Effects of TNF-α on autophagy of rheumatoid arthritis fibroblast-like synoviocytes and regulation of the NF-κB signaling pathway. Immunobiology. 2021;226(2):152059. https://doi.org/10.1016/j.imbio.2021.152059

8. Vomero M, Manganelli V, Barbati C, Colasanti T, Capozzi A, Finucci A, et al. Reduction of autophagy and increase in apoptosis correlates with a favorable clinical outcome in patients with rheumatoid arthritis treated with anti-TNF drugs. Arthritis Res Ther. 2019;21(1):39. https://doi.org/10.1186/s13075-019-1818-x

9. Grabiec AM, Angiolilli C, Hartkamp LM, van Baarsen LG, Tak PP, Reedquist KA. JNK-dependent downregulation of FoxO1 is required to promote the survival of fibroblast-like synoviocytes in rheumatoid arthritis. Ann Rheum Dis. 2015;74(9):1763-1771. https://doi.org/10.1136/annrheumdis-2013-203610

10. Zhao Y, Yang J, Liao W, Liu X, Zhang H, Wang S, et al. Cytosolic FoxO1 is essential for the induction of autophagy and tumour suppressor activity. Nat Cell Biol. 2010;12(7):665-675. https://doi.org/10.1038/ncb2069

11. Chen B, Wang F, Zhang Y, Liu F. PTEN-mediated FOXO signaling affects autophagy, migration and invasion of rheumatoid arthritis fibroblast-like synoviocytes. Tissue Cell. 2024;86:102278. https://doi.org/10.1016/j.tice.2023.102278

12. Zarnack K, König J, Tajnik M, Martincorena I, Eustermann S, Stévant I, et al. Direct competition between hnRNP C and U2AF65 protects the transcriptome from the exonization of Alu elements. Cell. 2013;152(3):453-466. https://doi.org/10.1016/j.cell.2012.12.023

13. Liu N, Dai Q, Zheng G, He C, Parisien M, Pan T. N(6)-methyladenosine-dependent RNA structural switches regulate RNA-protein interactions. Nature. 2015;518(7540):560-564. https://doi.org/10.1038/nature14234

14. Dominissini D, Moshitch-Moshkovitz S, Schwartz S, Salmon-Divon M, Ungar L, Osenberg S, et al. Topology of the human and mouse m6A RNA methylomes revealed by m6A-seq. Nature. 2012;485(7397):201-206. https://doi.org/10.1038/nature11112

15. Meyer KD, Saletore Y, Zumbo P, Elemento O, Mason CE, Jaffrey SR. Comprehensive analysis of mRNA methylation reveals enrichment in 3' UTRs and near stop codons. Cell. 2012;149(7):1635-1646. https://doi.org/10.1016/j.cell.2012.05.003

16. Wang X, Lu Z, Gomez A, Hon GC, Yue Y, Han D, et al. N6-methyladenosine-dependent regulation of messenger RNA stability. Nature. 2014;505(7481):117-120. https://doi.org/10.1038/nature12730

17. Song S, Zhao R, Qiao J, Liu J, Cheng T, Zhang SX, et al. Predictive value of drug efficacy by M6A modification patterns in rheumatoid arthritis patients. Front Immunol. 2022;13:940918. https://doi.org/10.3389/fimmu.2022.940918

18. Ma C, Wu J, Lei H, Huang H, Li Y. Significance of m6A in subtype identification, immunological evolution, and therapeutic sensitivity of RA. Immunobiology. 2024;229(1):152781. https://doi.org/10.1016/j.imbio.2023.152781

19. Wang F, Wen J, Liu J, Xin L, Fang Y, Sun Y, et al. Demethylase FTO mediates m6A modification of ENST00000619282 to promote apoptosis escape in rheumatoid arthritis and the intervention effect of Xinfeng Capsule. Front Immunol. 2025;16:1556764. https://doi.org/10.3389/fimmu.2025.1556764

20. Miyazawa K, Mori A, Okudaira H. Establishment and characterization of a novel human rheumatoid fibroblast-like synoviocyte line, MH7A, immortalized with SV40 T antigen. J Biochem. 1998;124(6):1153-1162. https://doi.org/10.1093/oxfordjournals.jbchem.a022233

21. Tasaki S, Suzuki K, Kassai Y, Takeshita M, Murota A, Kondo Y, et al. Multi-omics monitoring of drug response in rheumatoid arthritis in pursuit of molecular remission. Nat Commun. 2018;9(1):2755. https://doi.org/10.1038/s41467-018-05044-4

22. Ritchie ME, Phipson B, Wu D, Hu Y, Law CW, Shi W, et al. limma powers differential expression analyses for RNA-sequencing and microarray studies. Nucleic Acids Res. 2015;43(7):e47. https://doi.org/10.1093/nar/gkv007

23. Tominaga H, Ishiyama M, Ohseto F, Sasamoto K, Hamamoto T, Suzuki K, et al. A water-soluble tetrazolium salt useful for colorimetric cell viability assay. Anal Commun. 1999;36:47-50. https://doi.org/10.1039/A809656B

24. Kimura S, Noda T, Yoshimori T. Dissection of the autophagosome maturation process by a novel reporter protein, tandem fluorescent-tagged LC3. Autophagy. 2007;3(5):452-460. https://doi.org/10.4161/auto.4451

25. Kabeya Y, Mizushima N, Ueno T, Yamamoto A, Kirisako T, Noda T, et al. LC3, a mammalian homologue of yeast Apg8p, is localized in autophagosome membranes after processing. EMBO J. 2000;19(21):5720-5728. https://doi.org/10.1093/emboj/19.21.5720

26. Klionsky DJ, Abdel-Aziz AK, Abdelfatah S, Abdellatif M, Abdoli A, Abel S, et al. Guidelines for the use and interpretation of assays for monitoring autophagy (4th edition). Autophagy. 2021;17(1):1-382. https://doi.org/10.1080/15548627.2020.1797280

Statements and Declarations

Ethics approval and consent to participate

Not applicable. This study used a publicly available transcriptomic dataset and established cell lines and did not involve human participants or live animals.

Consent for publication

Not applicable.

Availability of data and materials

The public expression dataset is available in GEO under accession GSE93776. Source data and recalculated statistical results for the reported WB and CCK-8 analyses are supplied as supplementary files. Other experimental data are available from the corresponding authors upon reasonable request. Available uncropped blot images are supplied separately.

Competing interests

All authors certify that they have no affiliations with or involvement in any organization or entity with any financial interest or non-financial interest in the subject matter or materials discussed in this manuscript.

Funding

This work was supported by the Jiangxi Provincial Science and Technology Department Natural Science Foundation, Youth Fund Project 20242BAB20387.

Author Contributions Statement

Z.P.Z.: Investigation, Validation, Writing – Review & Editing.

B.W.Z.: Investigation, Methodology, Formal Analysis.

W.Y.: Writing – Original Draft, Visualization, Data Curation.

S.Y.G.: Resources, Validation.

Z.W.: Software, Formal Analysis.

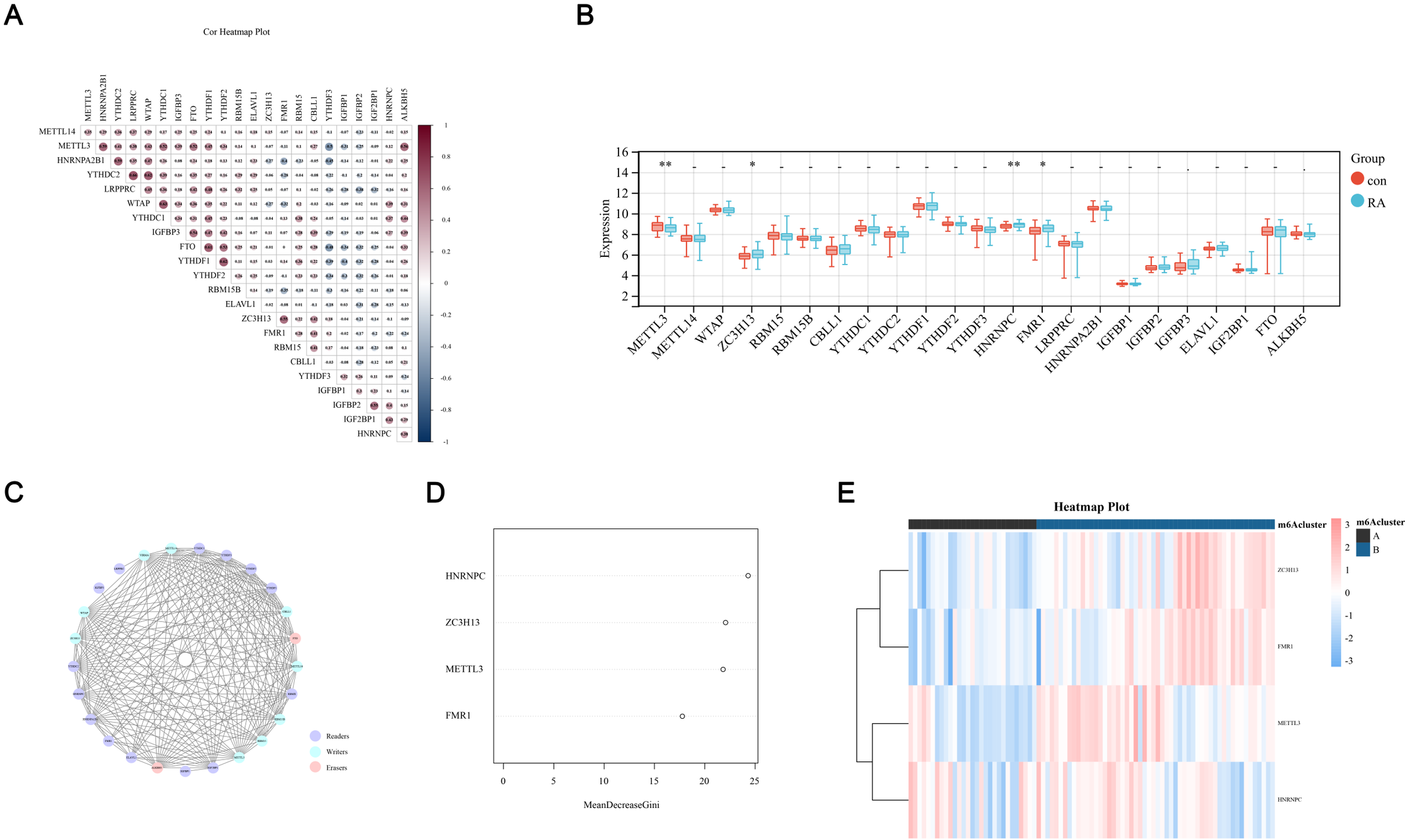
P.Y.: Supervision, Funding Acquisition, Writing – Review & Editing.

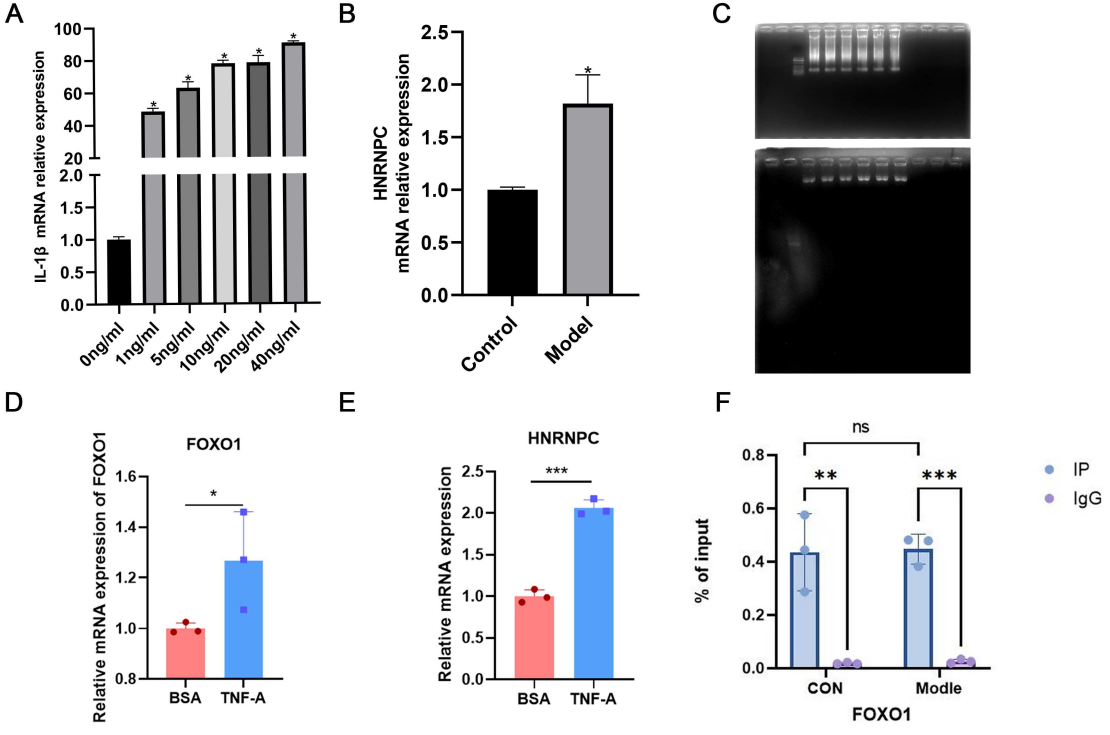
Z.B.X.: Conceptualization, Supervision, Project Administration, Funding Acquisition, Data Curation, Writing – Review & Editing.

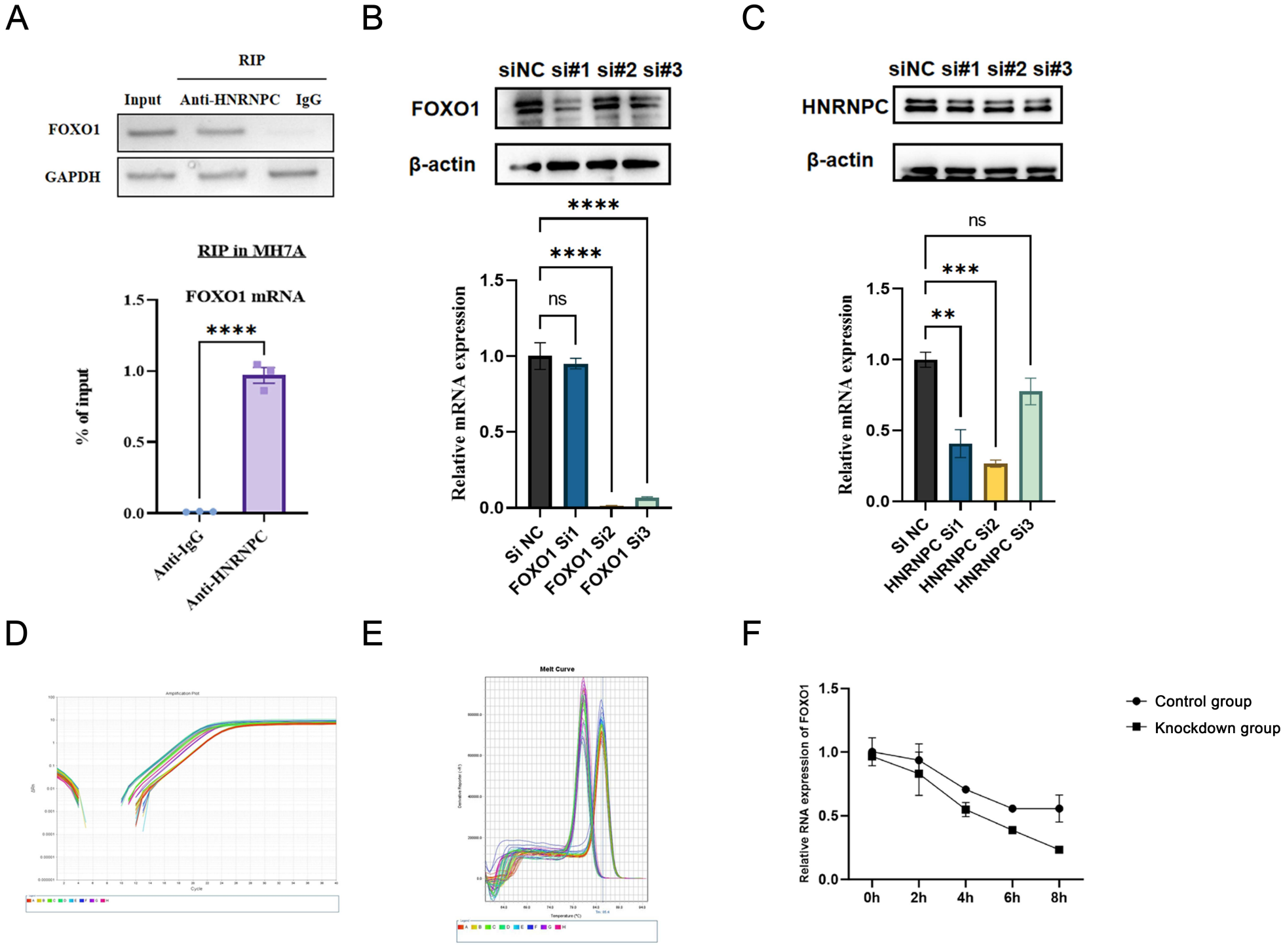
S.T.G.: Writing – Review & Editing.

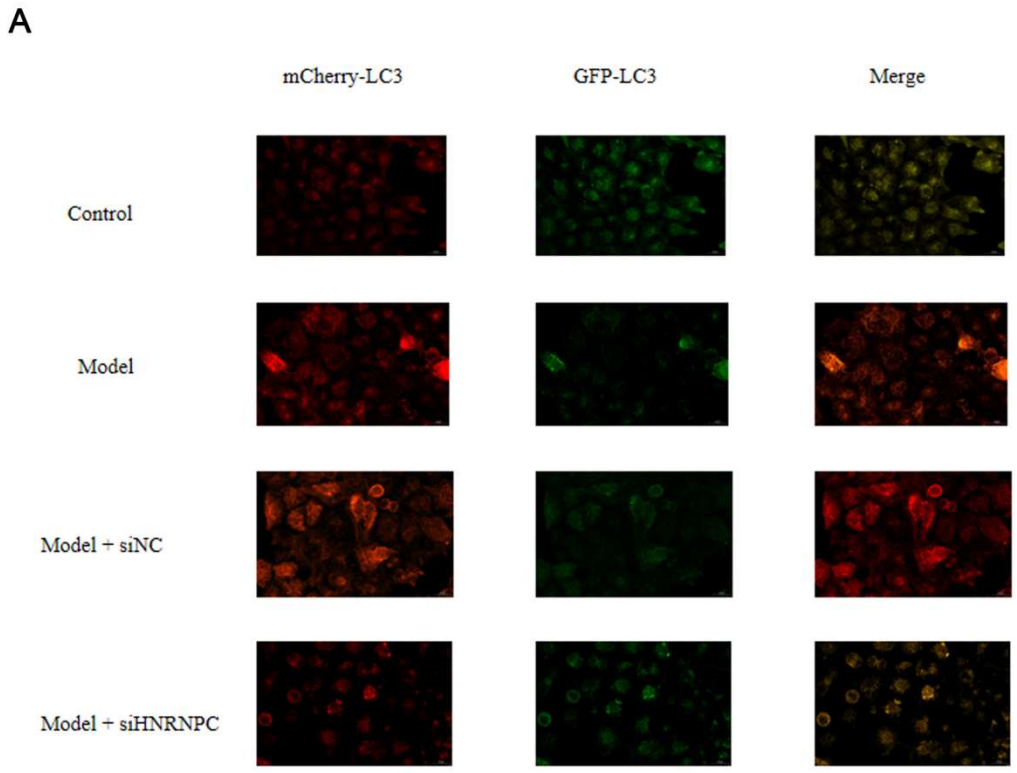
Use of AI-assisted tools

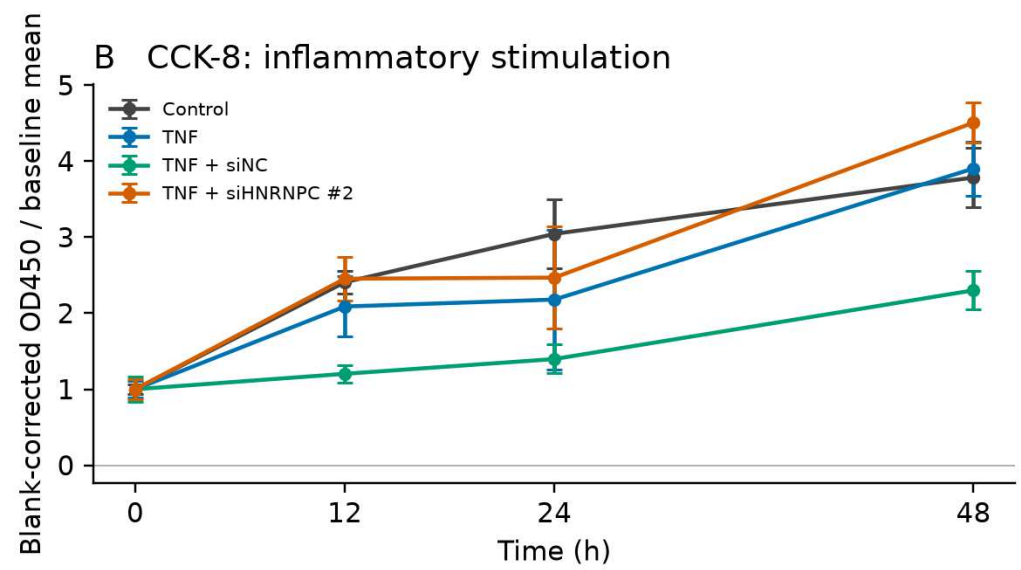
The authors used ChatGPT/Codex to assist with manuscript restructuring, language editing, and preparation of analysis scripts. Statistical calculations were executed locally on the supplied data. The authors are responsible for reviewing the analysis, verifying scientific statements, and approving the submitted manuscript.

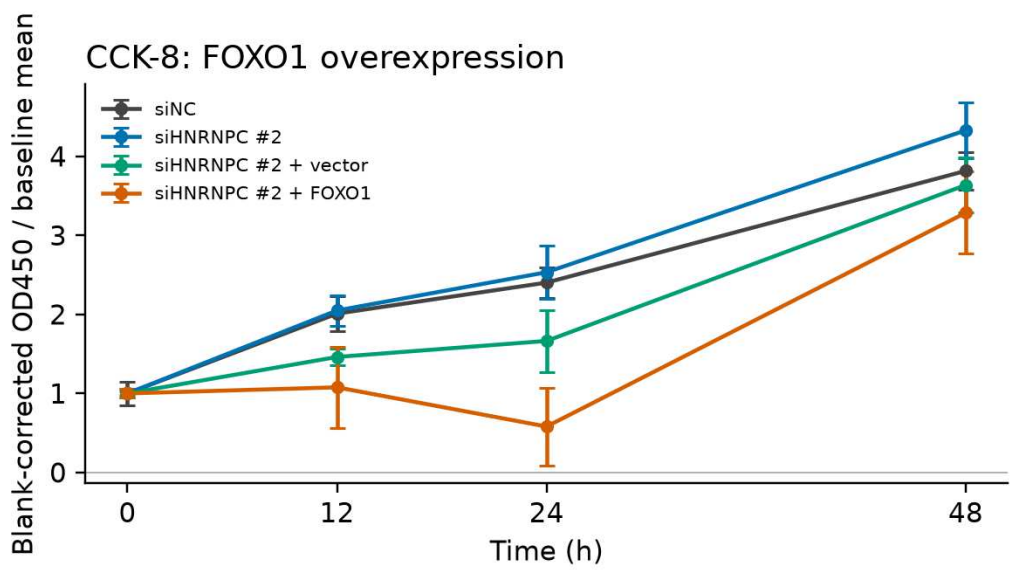

A
Cor Heatmap Plot
METTL3
HNRNPA2B1
YTHDC2
LRPPRC
WTAP
YTHDC1
IGFBP3
FTO
YTHDF1
YTHDF2
RBM15B
ELAVL1
ZC3H13
FMR1
RBM15
CBLL1
YTHDF3
IGFBP1
IGFBP2
IGF2BP1
HNRNPC
ALKBH5
METTL14
1
0.8
0.6
0.4
0.2
0
-0.2
-0.4
-0.6
-0.8
-1
B
Expression
16
14
12
10
8
6
4
2
**
*
Group
con
RA
METTL3
METTL14
WTAP
ZC3H13
RBM15
RBM15B
CBLL1
YTHDC1
YTHDC2
YTHDF1
YTHDF2
YTHDF3
HNRNPC
FMR1
LRPPRC
HNRNPA2B1
IGFBP1
IGFBP2
IGFBP3
ELAVL1
IGF2BP1
FTO
ALKBH5
C
Readers
Writers
Erasers
D
HNRNPC
ZC3H13
METTL3
FMR1
0
5
10
15
20
25
MeanDecreaseGini
E
Heatmap Plot
m6Acluster
A
B
3
2
1
0
-1
-2
-3
ZC3H13
FMR1
METTL3
HNRNPC

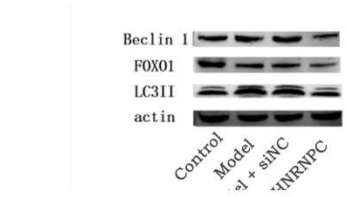

A
IL-1β mRNA relative expression
0ng/ml
1ng/ml
5ng/ml
10ng/ml
20ng/ml
40ng/ml
B
HNRNPC
mRNA relative expression
Control
Model
C
D
FOXO1
Relative mRNA expression of FOXO1
BSA
TNF-A
E
HNRNPC
Relative mRNA expression
BSA
TNF-A
F
ns
% of input
IP
IgG
CON
Modle
FOXO1

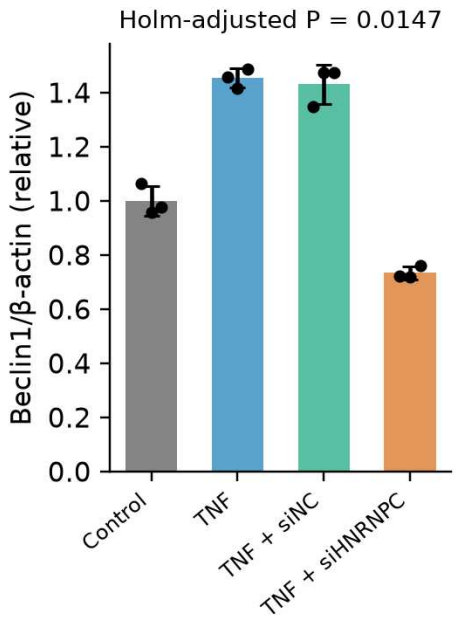

A
RIP
Input
Anti-HNRNPC
IgG
FOXO1
GAPDH
RIP in MH7A
FOXO1 mRNA
% of input
1.5
1.0
0.5
0.0
****
Anti-IgG
Anti-HNRNPC
B
siNC si#1 si#2 si#3
FOXO1
β-actin
****
****
ns
Relative mRNA expression
1.5
1.0
0.5
0.0
Si NC
FOXO1 Si1
FOXO1 Si2
FOXO1 Si3
C
siNC si#1 si#2 si#3
HNRNPC
β-actin
ns
***
**
Relative mRNA expression
1.5
1.0
0.5
0.0
SI NC
HNRNPC Si1
HNRNPC Si2
HNRNPC Si3
D
Amplification Plot
Cycle
E
Melt Curve
Temperature (°C)
F
Relative RNA expression of FOXO1
1.5
1.0
0.5
0.0
0h
2h
4h
6h
8h
Control group
Knockdown group

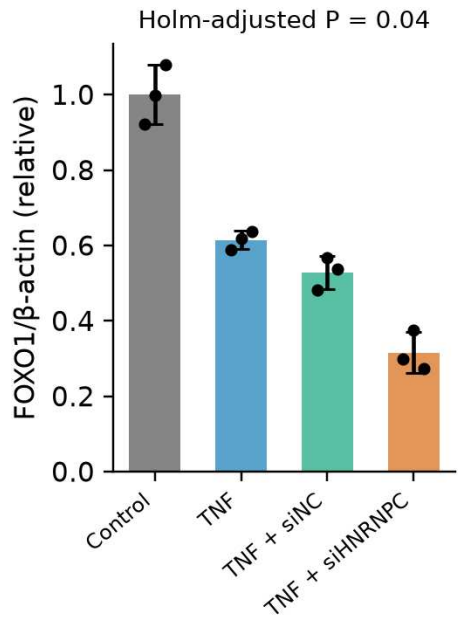

A
mCherry-LC3
GFP-LC3
Merge
Control
Model
Model + siNC
Model + siHNRNPC

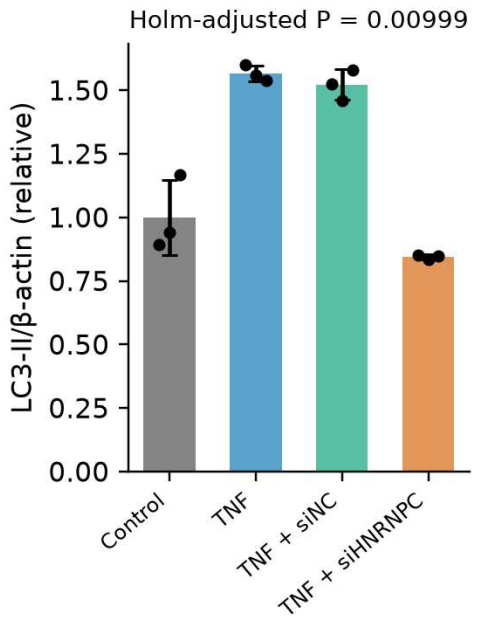

B CCK-8: inflammatory stimulation
Control
TNF
TNF + siNC
TNF + siHNRNPC #2
k-corrected OD450 / baseline mean
Blan
Time (h)

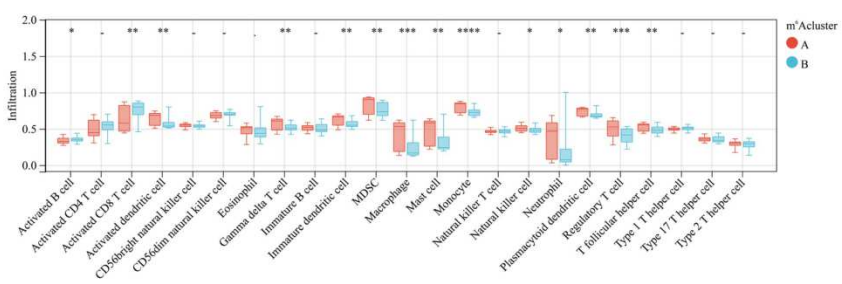

CCK-8: FOXO1 overexpression
siNC
siHNRNPC #2
siHNRNPC #2 + vector
siHNRNPC #2 + FOXO1
k-corrected OD450 / baseline mean
Blan
Time (h)


C
Beclin 1
FOXO1
LC3II
actin
Control
Model


Holm-adjusted P = 0.0147
Beclin1/β-actin (relative)
Control
TNF
TNF + siNC
TNF + siHNRNPC


Holm-adjusted P = 0.04
FOXO1/β-actin (relative)
Control
TNF
TNF + siNC
TNF + siHNRNPC


Holm-adjusted P = 0.00999
LC3-II/β-actin (relative)
Control
TNF
TNF + siNC
TNF + siHNRNPC


Infiltration
m6Acluster
A
B
Activated B cell
Activated CD4 T cell
Activated CD8 T cell
Activated dendritic cell
CD56bright natural killer cell
CD56dim natural killer cell
Eosinophil
Gamma delta T cell
Immature B cell
Immature dendritic cell
MDSC
Macrophage
Mast cell
Monocyte
Natural killer T cell
Natural killer cell
Neutrophil
Plasmacytoid dendritic cell
Regulatory T cell
T follicular helper cell
Type 1 T helper cell
Type 17 T helper cell
Type 2 T helper cell

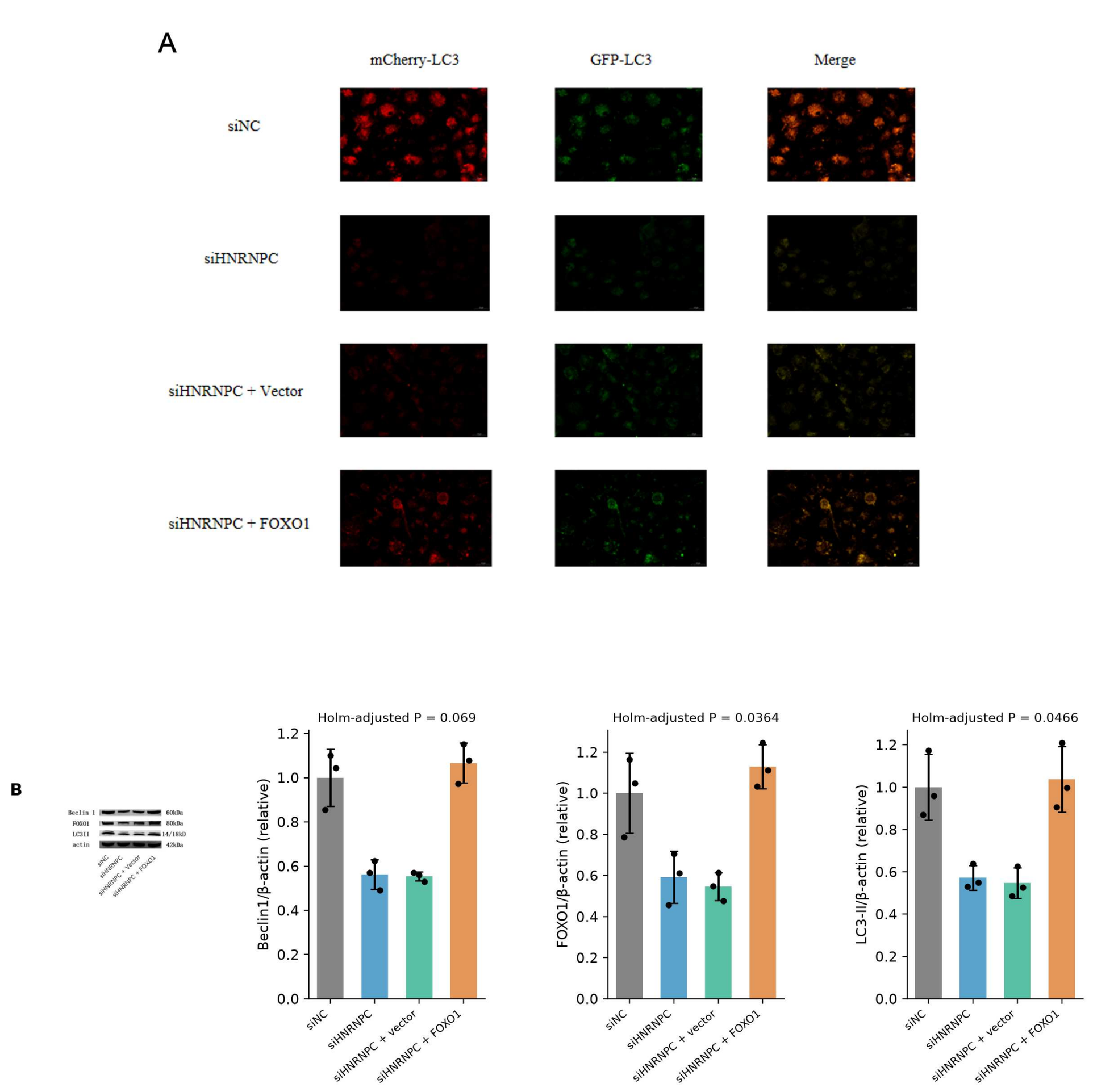

A
mCherry-LC3
GFP-LC3
Merge
siNC
siHNRNPC
siHNRNPC + Vector
siHNRNPC + FOXO1
B
Beclin 1
FOXO1
LC3II
actin
60kDa
80kDa
14/18kD
42kDa
siNC
siHNRNPC
siHNRNPC + Vector
siHNRNPC + FOXO1
Holm-adjusted P = 0.069
Beclin1/β-actin (relative)
Holm-adjusted P = 0.0364
FOXO1/β-actin (relative)
Holm-adjusted P = 0.0466
LC3-II/β-actin (relative)
0.0
0.2
0.4
0.6
0.8
1.0
1.2
siNC
siHNRNPC
siHNRNPC + vector
siHNRNPC + FOXO1

Figure Legends

Fig. 1. Exploratory public expression analysis prioritizes HNRNPC in RA

(A) Correlations and expression profiles of m6A-associated regulators. (B) Differential expression between RA and control samples. (C) STRING association network. (D) Random-forest feature importance. (E) Expression heatmap. (F) Expression-derived m6A-regulator scores and immune-related signatures. Public-data analyses were exploratory; scores do not directly measure RNA methylation or cell infiltration.

Fig. 2. HNRNPC and FOXO1 transcript expression and FOXO1 m6A enrichment

(A) IL1B transcript abundance across the TNF-α concentration series. (B) HNRNPC transcript abundance in control and model cells. (C) Electrophoretic images from the RNA-assay workflow. (D, E) FOXO1 and HNRNPC transcript abundance, respectively. (F) FOXO1 RNA enrichment in anti-m6A and IgG immunoprecipitates, expressed as percentage of input. FOXO1 RNA was enriched relative to IgG in both conditions, without a significant control–model difference in the analysis. Model stimulation was 20 ng/mL TNF-α for 48 h.

Fig. 3. HNRNPC-associated FOXO1 RNA and transcript decay

(A) FOXO1 RNA enrichment in anti-HNRNPC and IgG immunoprecipitates. (B) FOXO1-targeting siRNA screen. (C) HNRNPC-targeting siRNA screen. Panels B and C include protein and transcript measurements. si-FOXO1 #3 and si-HNRNPC #2 were selected from their respective screens. (D, E) qPCR amplification and melting curves. (F) FOXO1 RNA remaining at 0, 2, 4, 6, and 8 h after transcriptional inhibition in control and HNRNPC-depleted cells.

Fig. 4. LC3 reporter patterns, cell metabolic activity, and protein responses to HNRNPC depletion

(A) Representative tandem mCherry-GFP-LC3B reporter images. Images are qualitative; no puncta-count statistics were performed. (B) CCK-8 time courses for inflammatory stimulation and FOXO1 overexpression experiments, redrawn from the source values. Points show mean ± SD, n = 5 independent experiments. Readings were blank-corrected and normalized to the corresponding baseline-group mean. The negative blank-corrected observation was retained. CCK-8 comparisons used two-sided Welch t tests with Holm correction across eight tests per panel; exact P values are in Supplementary Statistical Tables. (C) Representative immunoblots and protein quantification, mean ± SD with individual observations, n = 3 independent experiments. Each run included all four groups. Target signals were normalized to β-actin and then to the mean control value. The displayed

P values compare model + siNC with model + siHNRNPC using paired t tests with Holm correction across six pairs per protein. (D) Public-data ssGSEA signature scores. siHNRNPC denotes si-HNRNPC #2. TNF-α: 20 ng/mL for 48 h.

Fig. 5. FOXO1 restoration partially reverses the autophagy-related effects of HNRNPC depletion

(A) Representative tandem mCherry-GFP-LC3B images in siNC, siHNRNPC, siHNRNPC + empty vector, and siHNRNPC + FOXO1-overexpressing cells. Images were assessed qualitatively without puncta-count statistics. (B) Representative immunoblots and quantification of Beclin1, FOXO1, and LC3-II. Signals were normalized to β-actin and expressed relative to the mean siNC ratio. Bars show mean ± SD with individual observations from three independent experiments, each containing all four groups. The displayed P values compare the empty-vector and FOXO1-overexpressing conditions using two-sided paired t tests with Holm correction across all six pairs per protein. Beclin1 did not reach significance after correction. siHNRNPC denotes si-HNRNPC #2. TNF-α: 20 ng/mL for 48 h.

Supplementary Files

This is a list of supplementary files associated with this preprint. Click to download.

- CCK8latestExceldescriptives.csv
- figureprocessingrecord.txt
- CCK8latestExcelstatistics.csv
- CCK8authorconfirmedsource.xlsx
- WBdescriptivestatistics.csv
- CCK8latestExcelvalues.csv
- SupplementaryStatisticalTables.docx
- WBfinalmatchedstatistics.csv
- WBfullprecisionvalues.csv
- SupplementaryStatisticalTables.pdf
- UncroppedWBSourceImages.pdf
- UncroppedWBSourceImages.docx
- actinr.tif
- Beclin1r.tif
- FOXO1r.tif
- LC3IIr.tif
- FOXO1.tif
- LC3II.tif
- Beclin1.tif
- actin.tif
- Beclin1r.tif
- actin.tif
- actinr.tif
- FOXO1.tif
- LC3II.tif
- Beclin1.tif
- FOXO1r.tif
- LC3IIr.tif